Optica Applicata, Vol. XV, No. 1, 1985

Prototype device design of Zn_3P_2-based solar cells*

JANUSZ M. PAWLIKOWSKI

Institute of Energy Conversion, University of Delaware, Newark DE 19716, USA, and Institute of Physics, Technical University of Wrocław, Poland **.

The photon collection and carrier collection efficiencies of prototype Zn_3P_2-based solar cell devices have been computed. The choice has been discussed of the device configuration, thickness of basic semiconductor, partner materials, doping levels and ohmic contacts. Finally, the short-circuit current gain and the total conversion efficiency have been calculated for Zn_3P_2-based solar cell and compared to the experimental data of prototype devices.

1. Introduction

The successful development of any solar cell can be traced through a number of distinct stages. In each of these stages certain modelling, computation and measurement procedures are essential to achieve any significant progress. The first step is to identify a possible semiconductor for the carrier generator and to establish its fundamental optical and electronic properties. Following that there come studies of photon economy, photon collection efficiency (i.e., the number of photons absorbed inside the semiconductor divided by the number of photons irradiating the sample), quantum efficiency of photo-generation (i.e., the ratio of photo-generated current carriers to the photons absorbed), carrier collection efficiency (i.e., the number of carriers collected at the terminals per one photo-generated carrier) and the total conversion efficiency (i.e., the power received per unit incident power) to select the prototype device configuration. The next stage is to produce and develop the prototype devices leading finally to a large-scale production technology. Four major stages of the solar cell development suggested here are presented in Table 1.

Recently, zinc phosphide (Zn_3P_2) has been intensively investigated as one of the high-efficiency semiconductors for solar cell applications. Some fundamental optical and electronic properties of Zn_3P_2 influencing a solar cell performance have been already reviewed in [1–3]. It is a goal of this paper to describe the second stage of the development of Zn_3P_2-based solar cell, focusing on the prototype device design.

---

* Work made in part under the contract sponsored by the Institute of Physics, Polish Academy of Sciences, Warsaw.

** Present address: Institute of Physics, Technical University of Wrocław, Wybrzeże Wyspiańskiego 27, 50-370 Wrocław, Poland.

Table 1. Major stages of solar cell development

Stage	Important studies	Main results
1st: Material studies	Optical and electronic properties	Choice of the semiconductor
2nd: Prototype device design	Photon economy	Choice of the configuration
	Photon and carrier collection efficiencies	
3rd: Prototype device development	Mechanical and chemical properties	Choice of the technology
	Stability and operation	Choice of the optimization trend
4th:	Large-scale production technology	

2. Device configuration

In the second stage of the solar cell development the choice has to be made of the device configuration: Schottky-type junction, homojunction or heterojunction. The choice is basically influenced by the diffusion length of minority carriers and the photon- and carrier-collection efficiencies, being in turn affected by electronic and optical properties of the semiconductor chosen as an absorber/generator. These properties are shortly described below.

The smallest energy bandgap of Zn_3P_2 has been ascribed to indirect transitions with onset at 1.315 eV and the fundamental absorption edge to direct transitions at the Γ point with onset at 1.51 eV, both at room temperature [4–6]. Absorption coefficient of Zn_3P_2 has been shown within a wide photon-energy range and found to be relatively high (of the order of $10^5\,cm^{-1}$) above the fundamental absorption edge [6]. A minority carrier (electrons) diffusion length has been estimated to be of the order of 2–10 μm by means of spectral response measurements [7, 8], electron beam induced current [9] and laser spot scanning [10] methods. A majority carrier (holes) lifetime of approximately 3 μsec has been estimated by means of photoconductivity measurements [11], which provides the values of 10–15 μm as a hole diffusion length. All samples of Zn_3P_2 measured so far have shown p-type conductivity over a temperature range of 80–380 K. The room-temperature resistivity lies usually between 10 and 200 ohm-cm, corresponding to the average value of hole concentration of $10^{22}\,m^{-3}$ and hole mobility of $(10–20)\times10^{-4}\,m^2/V$ sec [12]. Ionized impurity scattering at low temperatures and acoustic-photon scattering at high temperatures have been observed as the dominating mechanism [12, 13]. The surface recombination velocity has been found to dominate over the bulk one. The presence of grain boundaries does not appear to be detrimental to the bulk recombination. Crystal structure, thermal properties and some technological data concerning Zn_3P_2 are collected in [14].

Four practically possible device configurations have been taken here into considerations: (1) metal grid–Zn_3P_2 Schottky junction, (2) semitransparent metal–Zn_3P_2 Schottky junction, (3) p-n Zn_3P_2 homojunction, and (4) p-n Zn_3P_2 based heterojunction. In all the configurations the basic working-surface area of the device has been assumed to be 0.25 mm² and the device surface area taken as totalling 0.5 mm². *The metal grid–Zn_3P_2 device* arrangement is shown in Fig. 1a. Collecting dots (250 μm in diameter) with 25 μm-wide collecting bars are provided as terminals. The photo-current is collected by 5 μm-thick lines with 10 μm spacing for the electron diffusion length in Zn_3P_2 to be 5 μm, ap-

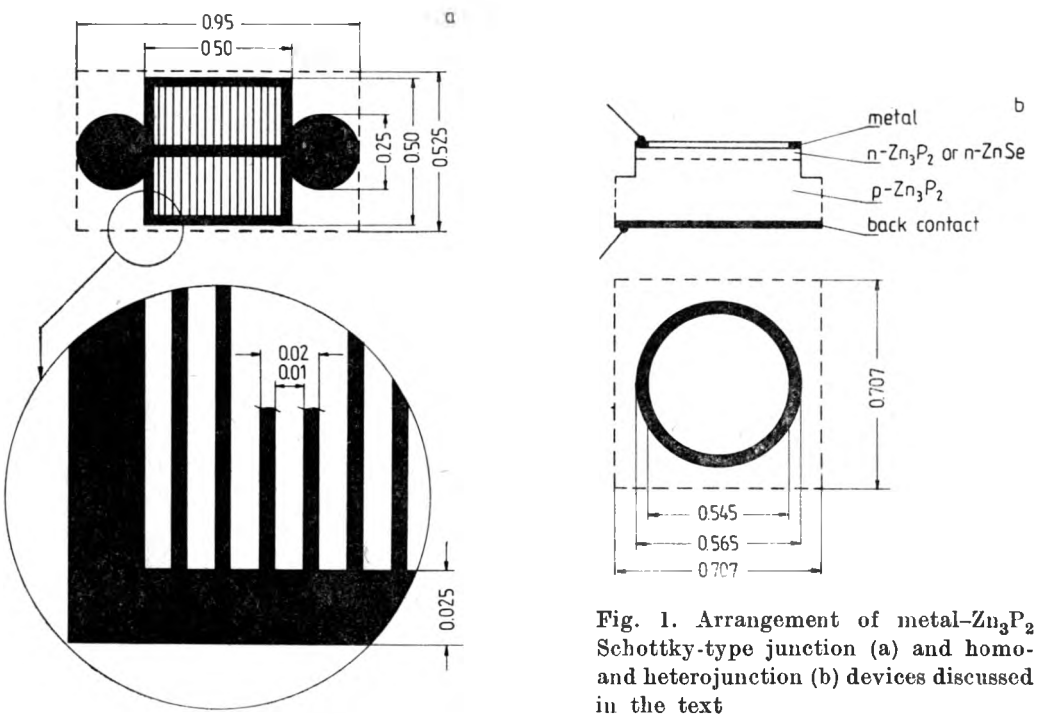

Fig. 1. Arrangement of metal–Zn_3P_2 Schottky-type junction (a) and homo- and heterojunction (b) devices discussed in the text

proximately. This arrangement provides the bare semiconductor-surface area equal to 0.1275 mm² and the one covered by the metal being equal to 0.1225 mm². Metal reflectivity coefficient of 97.5% has been assumed to be wavelength independent. *The semitransparent Mg–Zn_3P_2 device* arrangement is essentially the same as that in Fig. 1a having the collecting lines removed to reduce the reflection losses. Magnesium has been chosen as the barrier metal for the highest barrier on p-Zn_3P_2 achievable so far. The opaque metal surface (bar) screens 23.5% of the working area, the rest being covered by a 150 Å-thick magnesium film with transmittivity of $T \simeq 0.35$ and reflectivity of $R \simeq 0.50$. *The p-n junction device* arrangement is shown in Fig. 1b. Although the p-n junction formation in Zn_3P_2 has not been firmly proved so far, some evidence has been

discussed of forming a shallow p-n junction by Mg diffusion [15]. Therefore, this possibility is taken into considerations in the form of n-type front layer having the same optical properties as the p-type substrate, including relatively high optical losses on volume imperfections. A metal ring/bar 20μm wide is made of opaque metal leaving 86% of the semiconductor surface bare. 10 μm-deep junction has been assumed with diffusion to be the only effective mechanism of carrier transport towards the junction to build up the photo-current. *The ZnSe–Zn_3P_2 heterojunction device* arrangement is essentially the same as that for the p-n junction (Fig. 1b). A search for an appropriate heterojunction partner for Zn_3P_2 has been based on the energy bandgap, electron affinity, lattice constants and thermal properties, shortly reviewed in [3]. According to [3] ZnSe appears to be the best choice of the n-type partner for Zn_3P_2. Therefore, approximately 0.2 μm-thick ZnSe film has been assumed to be deposited on the top of Zn_3P_2 wafer with values of R and T taken from [16] in the region of interest. High level of absorption on the surface- and volume imperfections found in the ZnSe films in [16] has also been taken into account.

3. Photon collection efficiency

Taking the optical properties of Zn_3P_2, namely $T(\lambda)$ from [6] and $R(\lambda)$ from [4, 17], one can compute absorbance $A(\lambda) = 1 - R(\lambda) - T(\lambda)$ as the photon collection efficiency (PCE) of bare Zn_3P_2, under AM1.5 condition of illumination. In other words, only reflection losses from the bare Zn_3P_2 surface and transmission losses of photons escaped have been taken into account and the results set up the upper limit of the PCE, not achievable in the real devices, but useful in evaluating the material performance. Figure 2 shows $A(\lambda)$ versus wavelength

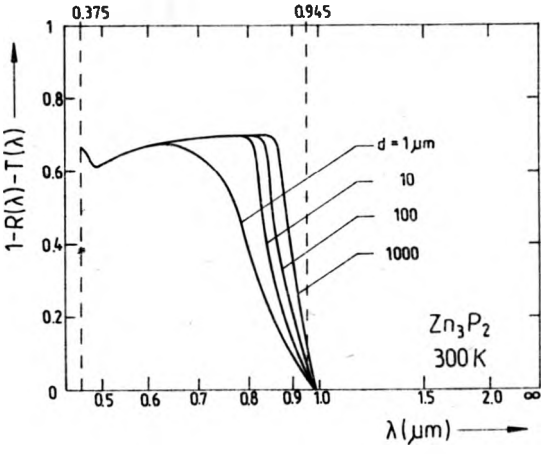

Fig. 2. Absorbance, $A = 1 - R - T$, of Zn_3P_2 wafers with thicknesses indicated. For explanation – see the text

for a few sample thicknesses taken as a parameter. The wavelength axis is distorted in this figure in accord with the integrated number of photons in the AM1.5 spectrum [18] up to the indicated wavelength. In this manner of presenta-

tion the ratio of the area under each curve to the total area of the figure is equal to the fraction of incident photons absorbed within the volume of Zn_3P_2 sample. The computed results of the upper limit of the PCE (in the sense given above) as a function of the wafer thickness are listed in Table 2. The values of 31 % and 65 % have been established as theoretical limits of the PCE at AM1.5 in the waverange of 0–∞ and 375–945 nm, respectively. The latter waverange has been chosen for the current generation processes in Zn_3P_2 taking place in this range effectively, in practice.

Table 2. Upper limit of the photon collection efficiency of Zn_3P_2-based devices under AM1.5 conditions

Zn_3P_2 thickness [μm]	PCE Per cent	
	375–945 nm waverange	0-∞ waverange
1	49.2	23.5
5	57.7	27.5
10	58.8	28.0
50	60.0	28.6
100	61.2	29.2
500	62.9	30.0
1000	64.3	30.6
very thick	≅ 65	≅ 31

The photon economy (i.e., the reflection and absorption losses as percentages of the incident photon flux) has been computed for the prototype device configurations considered above* and the results are shown in Figs. 3a–d. The results have been obtained for the very thick sample ($d \geqslant 1$ mm) and under AM1.5 condition of illumination integrated over 375–945 nm waverange. The differences in both absorption and reflection losses between the different configurations are distinctive and provide some notions on trends of optimization procedure. The values of generation gains for different device configurations, shown in Figs. 3a–d, represent the practical values of the PCE of the prototype devices with basic semiconductor being very thick. Although much lower than the upper limit of the PCE of bare Zn_3P_2, they also set up the upper limit of the PCE of the devices, for the thickness of Zn_3P_2 wafer is much smaller in practice (see below) than that assumed in the computations ($d \geqslant 1$ mm). The values of the PCE of prototype devices taken from Figs. 3a–d are listed in Table 3.

4. Quantum efficiency of photo-generation

Quantum efficiency (QE) of any photo-generation process, in which free carriers are produced by photons, is defined in practice as the ratio of the number of free electrons and/or holes to the number of photons absorbed in semiconductor.

* In the front-wall mode of operation – see below

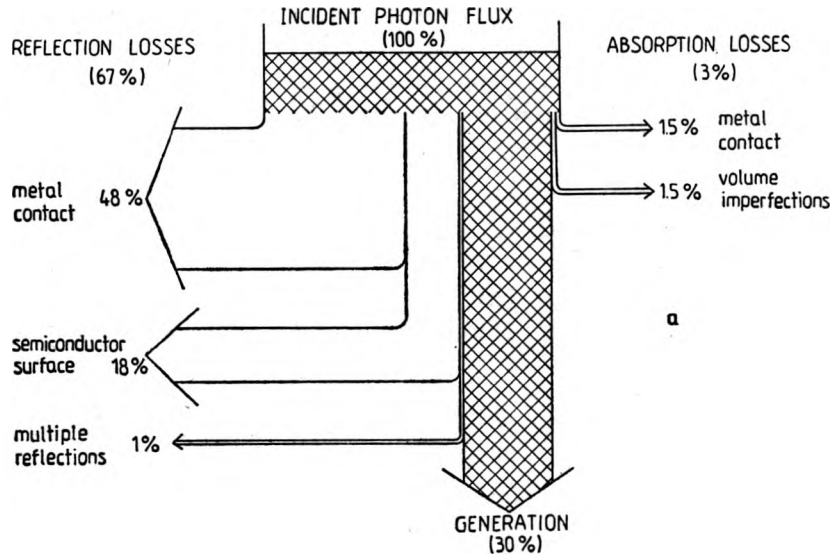
INCIDENT PHOTON FLUX
(100 %)
REFLECTION LOSSES
(67 %)
ABSORPTION LOSSES
(3%)
1.5 %
metal
contact
1.5 %
volume
imperfections
metal
contact
48 %
semiconductor
surface
18 %
multiple
reflections
1%
GENERATION
(30 %)

a

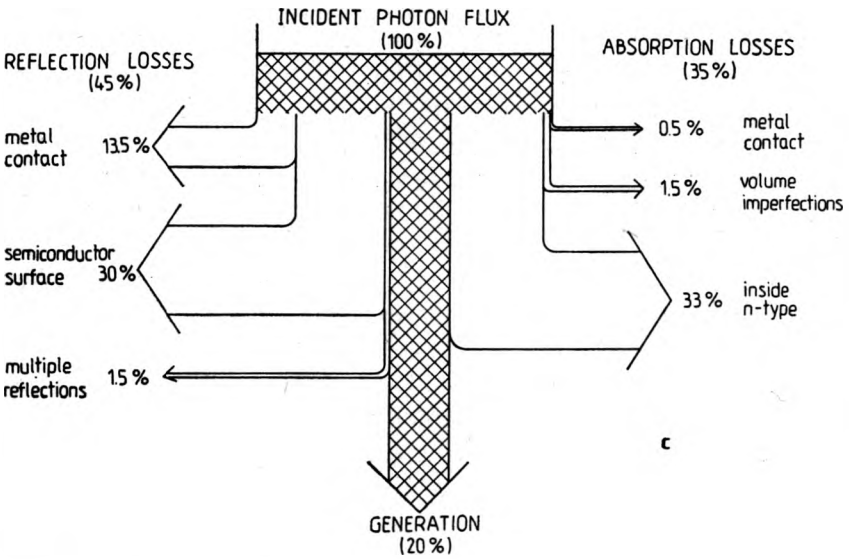
INCIDENT PHOTON FLUX
(100 %)
REFLECTION LOSSES
(45 %)
ABSORPTION LOSSES
(35 %)
0.5 %
metal
contact
1.5 %
volume
imperfections
33 %
inside
n-type
metal
contact
13.5 %
semiconductor
surface
30 %
multiple
reflections
1.5 %
GENERATION
(20 %)

c

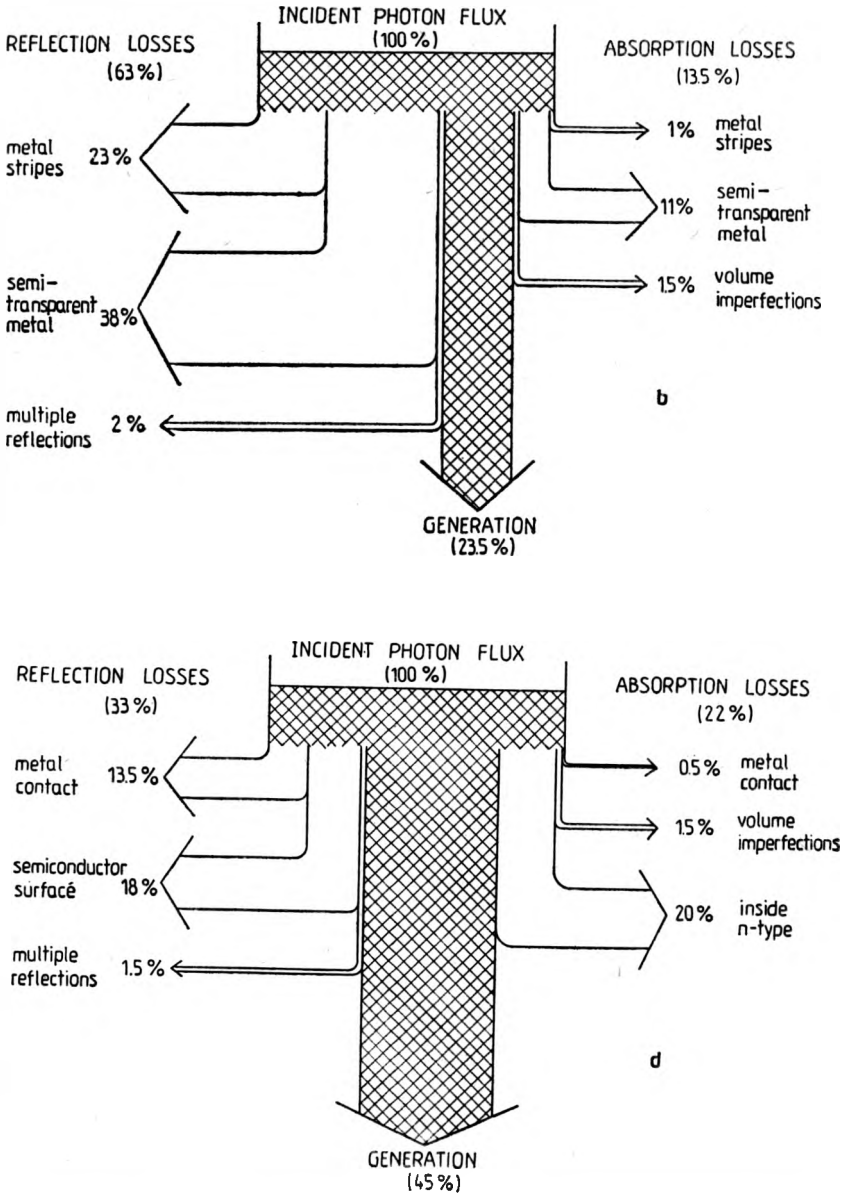

Fig. 3. Photon economy of metal grid–Zn_3P_2 Schottky junction (a), semitransparent Mg–Zn_3P_2 Schottky junction (b), n-on-p Zn_3P_2 homojunction (c), and ZnSe–Zn_3P_2 n-p heterojunction (d) solar cell devices

Table 3. Photon economy and collection efficiency of Zn_3P_2 based solar cells under AM1.5 illumination integrated over 375–945 nm waverange

Type of device	Reflection losses [%]	Absorption losses [%]	Photon collection efficiency [%]	Collected photon flux $[m^{-2}sec^{-1}]$
Metal grid-Zn_3P_2 Schottky junction	67	3	30	5.5×10^{20}
Semitransparent Mg-Zn_3P_2 Schottky junction	63 (54)*	13.5 (13)	23.5 (33)	4.3×10^{20} (6×10^{20})
Zn_3P_2 p-n homojunction	45	35	20	3.7×10^{20}
ZnSe-Zn_3P_2 heterojunction	33	22	45	8.3×10^{20}

* Assuming semitransparent metal to be 120 Å thick, instead of that of 150 Å

The results of measurements of the QE obtained in different semiconductors appear to be qualitatively similar, although the detailed shape of experimental curves may differ. For instance, the rise of the QE-versus-energy curve has been found (especially, in narrow-gap semiconductors) at photon energies, $\hbar\omega$, higher than double the energy gap due to the free-carrier multiplication process (see e.g. [25]).

There have been no detailed studies of the QE spectral characteristic of Zn_3P_2 yet. However, it seems to be reasonable to assume the value of the BA to be wavelength independent in the range of 375–945 nm and equal to unity, although QE > 1 is generally posssible for $\lambda < 300$ nm or under high electric field within the narrow and high potential barrier.

5. Carrier collection efficiency

The carrier collection efficiency (CCE) of heterojunction-type devices (Schottky-type junctions and ZnSe-Zn_3P_2 heterojunction) has been computed by means of the equation

$$(\mathrm{CCE})_{\mathrm{FW}} = \frac{aL_e}{a^2L_e^2 - 1} \frac{aL_e[\cosh(d/L_e) - \exp(-ad)] - \sinh(d/L_e)}{\cosh(d/L_e)} \tag{1}$$

for the front-wall (FW) mode of operation (light passes through the junction

region first, before entering the semiconductor substrate) and from the formula

$$(\mathrm{CCE})_{\mathrm{BW}} = \frac{aL_e}{a^2L_e^2-1}\,\frac{aL_e-\exp(-ad)[\sin h(d/L_e)+aL_e\cos h(d/L_e)]}{\cos h(d/L_e)} \tag{2}$$

for the back-wall (BW) mode (light is incident directly on the semiconductor before entering, if any, the junction region). The effect of the drift of carriers has been neglected, i.e., the junction region has been assumed to be negligibly narrow.

The CCE of homojunction-type devices has been computed by means of equation

$$(\mathrm{CCE})_{p-n} = (\mathrm{CCE})_n + (\mathrm{CCE})_p + (\mathrm{CCE})_j \tag{3}$$

where, for a shallow n-on-p homojunction [19],

$$(\mathrm{CCE})_n = \frac{aL_h}{a^2L_h^2-1}\left\{-aL_h\exp(-at) + \frac{SL_h+aL_h-\exp(-at)[SL_h\cos h(t/L_h)+\sin h(t/L_h)]}{SL_h\sin h(t/L_h)+\cos h(t/L_h)}\right\} \tag{4}$$

is the contribution from n-type region,

$$(\mathrm{CCE})_p = (\mathrm{CCE})_{\mathrm{FW}}\exp[-a(t+w)] \tag{5}$$

is the contribution from p-type region (where $(\mathrm{CCE})_{\mathrm{FW}}$ is given by Eq. (1)), and

$$(\mathrm{CCE})_j = \exp(-at)[1-\exp(-aw)] \tag{6}$$

is the contribution from the junction (built-in-field) region. In Equations (1)–(6) a is an absorption coefficient of semiconductor; L_e and L_h are diffusion lengths of electrons in p-type and holes in n-type, respectively; d, t and w are thicknesses of p-type, n-type and built-in-field regions, respectively; and S is a ratio of the surface recombination velocity to the hole diffusion coefficient in n-type region. Equations (4) and (5) have been obtained for diffusion in n-type and p-type regions to be dominated in minority carrier transport. In the computations, $a(\lambda)$ was taken from [6] and $L_e = 6\,\mu\mathrm{m}$ from [7–10]; and $L_h = 3\ \mu\mathrm{m}$, $t = 3\ \mu\mathrm{m}$, $d = 6\ \mu\mathrm{m}$ and $w = 1\ \mu\mathrm{m}$ were assumed according to the best knowledge and belief. The value of S has been estimated here as equal to $100\ \mathrm{cm}^{-1}$.

The spectral dependences of the CCE have been computed for the Zn_3P_2-based devices and are shown in Figs. 4a, b for the data listed above. Figure 4a shows the comparison of the plots in front-wall and back-wall configurations of heterojunction-type devices. The advantage of the FW mode is clearly seen, even in case of relatively thin semiconductor wafer considered. One-order-of-magnitude thicker sample makes this difference even more dramatic (broken line in Fig. 4a). Note, however, higher optical losses in the FW mode of operation (approximately double the optical losses in the BW mode of operation). Actually, technology has been influencing the choice of the FW or BW mode perhaps

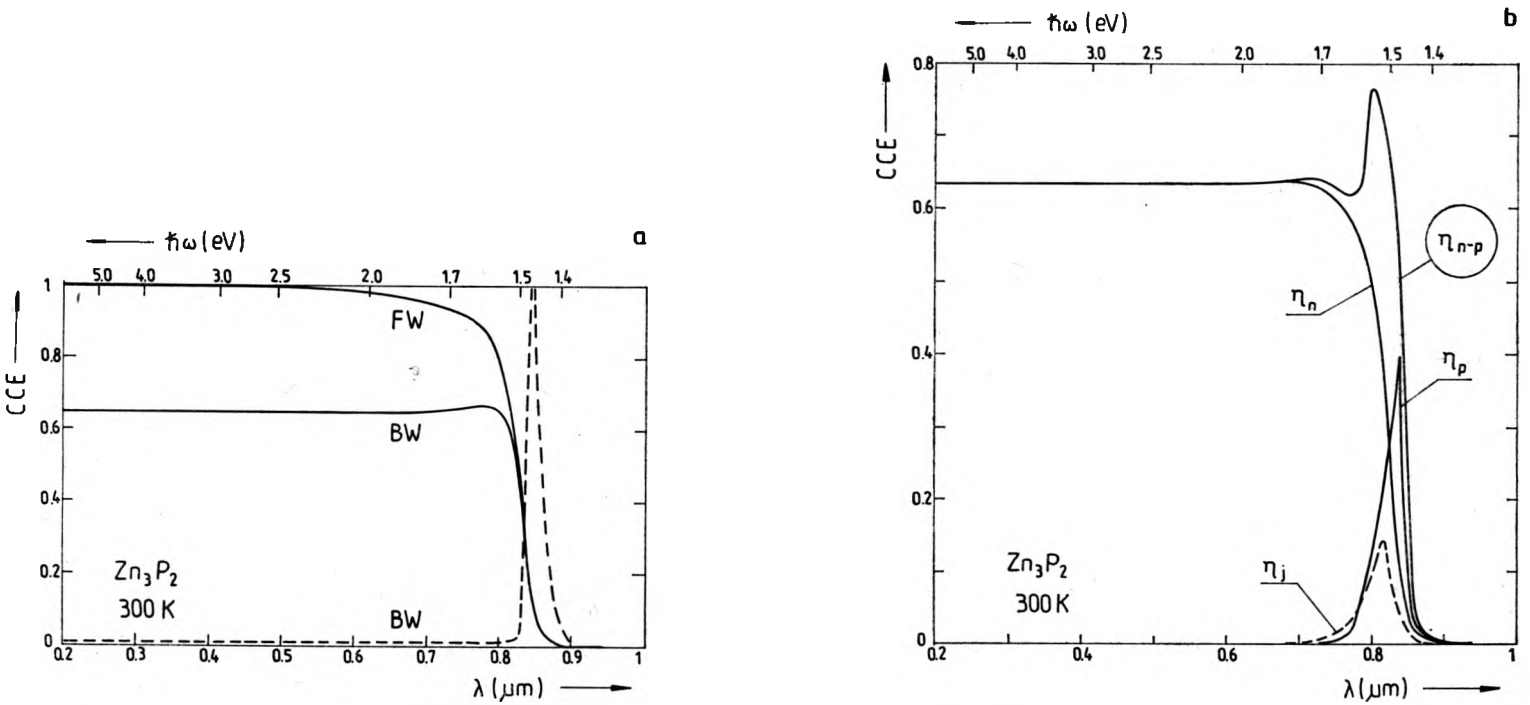

Fig. 4. Carrier collection efficiency of (a) heterojunction-type 6 μm-thick Zn_3P_2-based solar cell in the front-wall (FW) and back-wall (BW) configurations, for the parameters discussed in the text (dashed line shows the result for 60 μm-thick devices and is multiplied by 100); and (b) n-on-p homojunction 6 μm-thick-Zn_3P_2 device, for the parameters discussed in the text (notations η_{n-p}, η_n, η_p, and η_j correspond to the values computed from Eqs. (3)–(6), respectively

even more than the difference between the CCE's and has been making the FW mode to be more common. Similar results have been obtained for homojunction-type devices (Fig. 4b). The dominant part in total CCE of p-n junction has been taken by the front-wall layer of n-type (note that $t = L_h$) and the contribution of p-type region becomes dominant for $t \to 0$ and $w \to 0$ (see also Eq. (5)).

6. Overall collection efficiency

The overall collection efficiency (OCE) is defined here as the number of carriers collected at the terminals per one photon irradiating the device and its spectral plot is simply given by

$$(\mathrm{OCE})_\lambda = (\mathrm{PCE})_\lambda (\mathrm{QE})_\lambda (\mathrm{CCE})_\lambda . \tag{7}$$

Since the spectral plots of the PCE and CCE have been computed and the QE assumed to be equal to unity, the spectral curves of the OCE have been easily calculated for Zn_3P_2-based devices. Exemplary curves of the OCE for the metal grid-Zn_3P_2 Schottky junction, n-on-p homojunction and ZnSe-Zn_3P_2 heterojunction devices are shown in Fig. 5 (all in the FW mode of operation). They

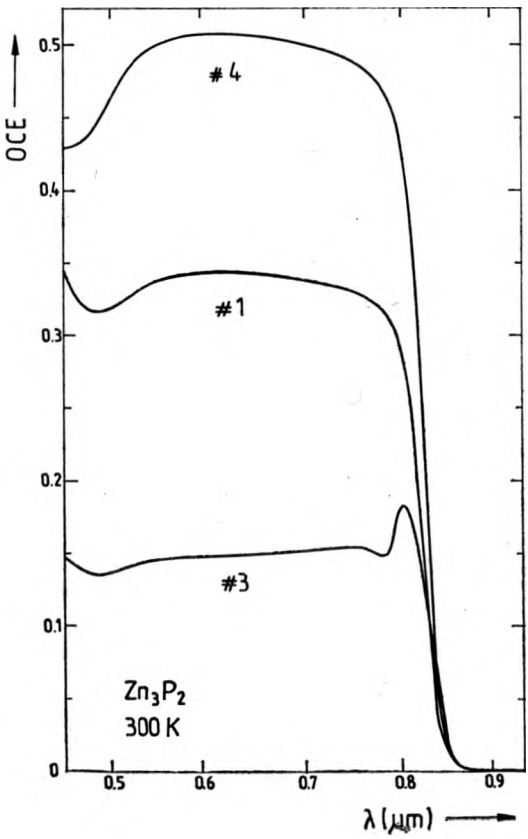

Fig. 6 ▼

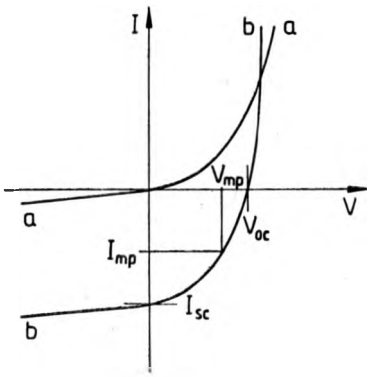

Fig. 5. Overall collection efficiency of metal grid-Zn_3P_2 junction (# 1) n-on-p homojunction (# 3), and ZnSe–Zn_3P_2 heterojunction (# 4) devices, for parameters discussed in the text

Fig. 6. Schematic I–V plots of dark (a) and illuminated (b) solar cell device

have been calculated for 6 μm-thick Zn_3P_2 wafer assumed. The differences of the PCE and CCE between different types of the devices cumulate here just giving the OCE of ZnSe-Zn_3P_2 heterojunction device to be approximately 3 times higher than that of p-n homojunction one; with Schottky-type devices being about in between. The significant drop on high-energy side in heterojunction device is due to an increase of optical losses in the ZnSe film. The calculated data of the PCE, CCE and OCE for 6 μm-thick Zn_3P_2 base under AM1.5 irradiation integrated over 375–945 nm waverange are listed in Table 4. The results for bare Zn_3P_2 are also included for comparison. Note the reduced values of the PCE comparing to those in Table 3; the latter being computed for a thick Zn_3P_2 base.

Table 4. Comparison of the design computation data and the experimental results for Zn_3P_2-based solar cells under AM1.5 illumination integrated over 375–945 nm waverange, in the FW mode

Type of device	PCE [%]	CCE [%]	OCE [%]	j_{sc} [A/m^2]	Upper limit of j_{sc}* [A/m^2]	Experimental data of j_{sc} [A/m^2]	
Metal grid-Zn_3P_2 Schottky junction	26.7	86.3	23.0	67.8	78.8	72	[20]
Semitransparent Mg-Zn_3P_2 Schottky junction	29.4	86.3	25.4	75.0	97.4	87	[21]
Zn_3P_2 p-n homojunction	17.8	60.0	10.7	31.6	52.5		
ZnSe-Zn_3P_2 heterojunction	40.0	86.3	34.6	102	118	37.5	[24]
Bare Zn_3P_2	58	100	58	1.07×10^{21} [photons / m^2 sec] = 172 A/m^2			

* Based on the PCE only, i.e., for CCE = 100%

7. Total conversion efficiency

The total conversion efficiency (TCE) is defined as the ratio of the power received P_r from the solar cell device to the incident power of solar spectrum P_i and is written as

$$\mathrm{TCE} = \frac{P_r}{P_i} = \frac{j_{sc} V_{oc} \mathrm{FF}}{P_i} \tag{8}$$

per unit area of the device, where j_{sc} is the short-circuit current from the device, V_{oc} is the open-circuit voltage between the terminals, and FF is the fill factor defined as

$$\mathrm{FF} = \frac{j_{mp} V_{mp}}{j_{sc} V_{oc}} \tag{9}$$

where j_{mp} and V_{mp} are the density of current and voltage in the point of I–V curve of maximal power received by an external receiver, respectively. Figure 6 shows an exemplary I–V curve of dark and illuminated solar cell and explains the parameters considered above. The values of j_{sc} have been computed by means of simple integration

$$j_{sc} = q \int_{\lambda_2}^{\lambda_1} \Phi(\lambda) \mathrm{OCE}(\lambda) d\lambda \tag{10}$$

where Φ is an incident photon flux within the waverange of interest. The valuse of j_{sc} of the devices considered are listed in Table 4. The upper limit of j_{sc} ever achievable in the devices considered (only when CCE = 100%, i.e. there are no current carrier lossses) is also listed in Table 4 for comparison. Although unrealistic, the j_{sc} from bare Zn_3P_2 is also included into Table 4 giving the notion on the highest *ever-thinkable* current output from 6 μm-Zn_3P_2-based solar cell devices.

To compute the TCE values, the fill factor value has been assumed to be equal to 0.5 and qV_{oc} has been taken as equal to $0.5\,E_g \cong 0.75$ eV. Computed values of the TCE are listed in Table 5. There are three sets of data: (i) the TCE of *working area* taking the upper limit of j_{sc} under considerations, (ii) the TCE of

Table 5. Total conversion efficiency (in per cent) of Zn_3P_2-based solar cells under AM1.5 illumination integrated over two waveranges indicated

Type of device	Working area, upper limit*		Working area		Total area	
	375–945 nm	0–∞	375–945 nm	0–∞	375–945 nm	0–∞
1. Metal grid-Zn_3P_2 Schottky junction	7.45	3.55	6.41	3.05	3.20	1.53
2. Semitransparent Mg-Zn_3P_2 Schottky junction	9.20	4.38	7.09	3.38	3.54	1.69
3. Zn_3P_2 p-n homojunction	4.96	2.36	2.99	1.42	1.49	0.71
4. ZnSe-Zn_3P_2 heterojunction	11.2	5.31	9.64	4.59	4.82	2.29
Bare Zn_3P_2	16.3	7.74				

* See Table 4 for upper limit of j_{sc}

working area taking the realistic values of j_{sc}, and (iii) the TCE of *total area* *Working area* means here the area of the barrier irradiated by solar beam, i.e.. 0.25 mm² in the devices considered. *Total area* is here equal to the total surface area of semiconductor used to prepare the device, i.e., 0.5 mm². In this sense, the working-area TCE describes the potential of the device and the total-area TCE sets up the output gain from the material used, important for the comercial

purposes too. Note that the TCE decreases effectively when solar cells are connected into modules and even further when modules form an array. Ten-to-twenty per cent decrease is expected of power output of the array comparing to that of the cells used.

8. Final comments

There are the experimental data available of the j_{sc}, under AM1.5 conditions, of prototype Zn_3P_2-based devices [20–24] which can be compared with the design computations (see Table 4). Magnesium Schottky-barrier grid devices have exhibited the total-area j_{sc} up to 72 A/m^2 [20], while semitransparent Mg-on-Zn_3P_2 devices have provided the total-area j_{sc} up to 87 A/m^2 [21]. The latter devices have been subsequently improved; the total-area j_{sc} up to 170 A/m^2 has been achieved [22] by means of AR coating which reduces the optical losses down to $\simeq 30$ per cent. Heating the Mg-Zn_3P_2 Schottky devices has been suggested to produce the p-n junction and the total-area j_{sc} up to 153 A/m^2 has been reported in the junctions with AR coating [23]. In thin film ZnSe-Zn_3P_2 heterojunction devices the total-area j_{sc} has been measured up to 37.5 A/m^2 only [24]. The strong recombination at the ZnSe/Zn_3P_2 interface has been suggested to be responsible for the current losses.

In conclusion, the experimental data of j_{sc} are quite close to these from design calculations, except for the heterojunction devices, just leaving the potential in development of this type of devices. However, the heterojunction devices have suffered, in principle, the relatively high level of recombination losses at the interface (not accounted for in the model) and the problem with n-type doping of ZnSe layer growing on the top of Zn_3P_2 has not been solved successfully, so far [16, 24]. Also, taking into consideration the apparent difficulty in obtaining the p-n homojunction in Zn_3P_2, the metal–Zn_3P_2 Schottky-type devices emerge as the best choice of the device type, actually. Note that the photon economy (hence, the PCE, and so on) in the semitransparent metal–Zn_3P_2 device is very sensitive to the thickness of the metal used. A change of the thickness of Mg layer from 150 Å to 120 Å (of the order of probable experimental error) provides the gain increase by 10 per cent, approximately (see Table 3). Nevertheless, the semitransparent metal-Zn_3P_2 device seems to be the best configuration, being also technologically superior to the metal grid–Zn_3P_2 one.

Taking 50 ohm-cm as an average value of the room-temperature resistivity of the large-grain polycrystalline Zn_3P_2 wafer (see Sec. 2) the series resistivity of 0.25 mm^2-in-area device is plotted in Fig. 7 as a function of Zn_3P_2 thickness. Note that the contact resistance influences the total series resistance of the device. This effect is strong in the thin film devices, especially, for the semiconductor resistance is then of a little importance. To make a low-resistivity ohmic contact with Zn_3P_2 is still an apparent problem and silver seems to be the best choice [26, 27]. To decrease the R_S, a moderate doping by Ag has been widely used providing with $N_A \simeq 10^{16}$ cm^{-3}. The search for the highest-barrier metal

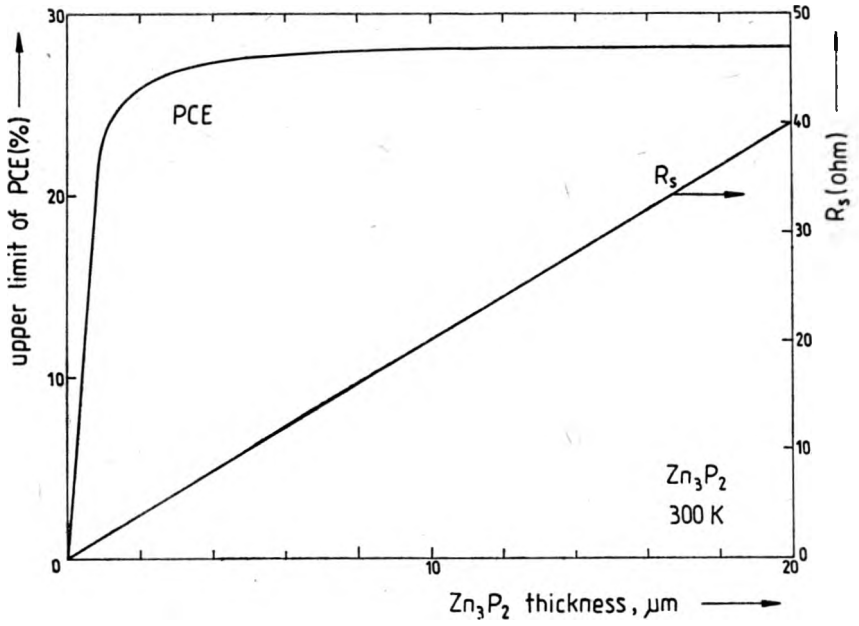

Fig. 7. Upper limit of the photon collection efficiency (PCE) and the series resistance (R_S) of Zn_3P_2 vs. the sample thickness

for Schottky-type devices has been conducted and magnesium has been established to be the best choice [27].

The unavoidable sequence of calculations of the efficiencies must be emphasized from: **PCE** (how many irradiating photons are captured ?), **QE** (how many carriers are they producing ?) and **CCE** (how many carriers produced will get to terminals ?) to **OCE** (how many carriers are eventually collected per one irradiating photon ?) and, finally, **TCE** (how good is the diode used as a converter/solar cell ?). In each of these steps, except **QE**, the efficiency is always lower than 100 per cent. The highest losses are due to the fundamental properties of semiconductor-class materials used as an absorber/generator: (1) some 30 per cent of the solar energy is reflected back from the semiconductor surface, (2) a portion of the solar spectrum (the infrared) is incapable of providing the minimum energy needed to release an electron/hole and is therefore unusable, and (3) all of the excess energy of the photons absorbed (energy above E_g, the minimum required) is converted into heat thus being lost inevitably. Moreover, any change in the semiconductor that reduces one of the last two losses necessarily worsens the other. A careful balance must be achieved between the two, thus limiting the choice of semiconductor. The second source of the high conversion losses is the electrical performance of the diode (built-in electric field in unavoidable part of the solar cell device). Although fill factors up to 0.83 [29] and 0.86 [30] have been discussed, most of the actually available devices has reached FF = 0.5–0.7. Also, V_{oc} has never reached the values predicted by simple estimations (i.e., $qV_{oc} \cong qU_D \cong E_g$ in p-n junction).

The total-area TCE of 1.53–1.69 per cent of the Zn_3P_2 Schottky-type junctions under AM1.5 irradiation integrated over $0-\infty$ waverange can be achieved at most, as it has emerged from Table 5. Although the TCE seems to be low, its value places Zn_3P_2 among the semiconductors suited very well for the solar cell applications. The unreliable data of the conversion efficiency, higher than 20 per cent, of the semiconductor with $E_g \cong 1.5$ eV published a few years ago (see, e.g., [28]) must not be treated seriously to be the TCE in the $0-\infty$ waverange of the real solar cell device with no AR coating.

There are some trends of optimization of the Zn_3P_2-based solar cells one can easily point out; to decrease the R_S value (the contact resistance mainly) and to apply effective AR coating are the first among them. The experimental research on it is currently under some progress.

Acknowledgements – Substantial part of this work was done under contract sponsored by the Solar Energy Research Institute, Golden, Colorado. The fruitful discussions with Drs M. Bhushan, A. W. Catalano and J. D. Meakin are greatfully acknowledged.

References

[1] ŻDANOWICZ W., ŻDANOWICZ L., Ann. Rev. Mater, Sci. **5** (1975), 301.
[2] PAWLIKOWSKI J. M., Infrared Phys. **21** (1981), 181.
[3] BHUSHAN M., PAWLIKOWSKI J. M., PEREYRA I., *Proc. of 161st Meeting of the Electrochemical Soc.*, Montreal 1982, Vol. 82–8, 1982, p. 505.
[4] PAWLIKOWSKI J. M., MISIEWICZ J., MIROWSKA N., J. Phys. Chem. Sol. **40** (1979), 1027.
[5] PAWLIKOWSKI J. M., J. Appl. Phys. **53** (1982), 3639.
[6] PAWLIKOWSKI J. M., Phys. Rev. **B26** (1982), 4711.
[7] CONVERS WYETH N., CATALANO A. W., J. Appl. Phys. **50** (1979), 1403.
[8] NAUKA K., MISIEWICZ J., Phys. Status Sol. **b65** (1981), K95.
[9] SUNDSTROM B. O., NILSON N. G., HULDT L., *Proc. of 1st Intern. Symp. on Phys. and Chem. of II–V Compounds*, Mogilany 1980, Eds. M. J. Gelten, L. Ždanowicz, Eindhoven 1980, p. 175.
[10] CATALANO A. W., MASI J. V., CONVERS WYETH N., *Proc. of 2nd E. C. Photovoltaic Solar Energy Conf.*, Berlin 1979, Ed. Riedel, Dordrecht, 1979, p. 440.
[11] WANG F.-C., Doctor's Thesis, Stanford University, 1982, unpublished.
[12] WANG F.-C., FAHRENBRUCH A. L., BUBE R. H., *Proc. of 15th IEEE Photovoltaic Specialists Conf.*, Orlando 1981, p. 1265.
[13] WANG F.-C., FAHRENBRUCH A. L., BUBE R. H., J. Electron, Mat. **11** (1982), 75.
[14] ARUSHANOV E. K., Prog. Crystal Growth Charact. **3** (1981), 211.
[15] CATALANO A. W., BHUSHAN M., Appl. Phys. Lett. **37** (1980), 567.
[16] PAWLIKOWSKI J. M., Thin Solid Films, 1985 (in press).
[17] MISIEWICZ J., Doctor's Thesis, Technical University of Wrocław, 1979, unpublished.
[18] *Terrestrial Photovoltaic Measurements Procedure*, NASA TN 73707; NASA-Lewis Research Center, Cleveland, Ohio, June 1977, p. 11.
[19] FAN J. C. C., BOZLER C. O., PALM B. J., Appl. Phys. Lett. **35** (1979), 875.
[20] CATALANO A. W., BHUSHAN M., CONVERS WYETH N., *Proc. of 14th IEEE Photovoltaic Specialists Conf.*, San Diego 1980, p. 641.
[21] BHUSHAN M., CATALANO A. W., *Proc. of 15th IEEE Photovoltaic Specialists Conf.*, Orlando 1981, p. 1261.
[22] BHUSHAN M., Appl. Phys. Lett. **40** (1982), 51.

[23] Bhushan M., J. Appl. Phys. **53** (1982), 514.
[24] Bhushan M., Pawlikowski J. M., in preparation.
[25] Scharoch P., Pawlikowski J. M., J. Appl. Phys. **55** (1984), 1487.
[26] Mirowska N., Doctor's Thesis, Technical University of Wrocław, 1984, unpublished.
[27] Convers Wyeth N., Catalano A. W., J. Appl. Phys. **51** (1980), 2286.
[28] Wysocki J. J., Rappaport P., J. Appl. Phys. **31** (1960), 571.
[29] Lindmayer J., Allison J., Tech. Rev. **3** (1973), 1.
[30] Wolf M., Energy Conversion **11** (1971), 63.

Received June 21, 1984

Проектирование первообразных солнечных батарей, основанных на Zn_3P_2

Расчитана производительность собрания фотонов и производительность собрания генерированных носителей в солнечных батареях, основанных на Zn_3P_2. Обсужден подбор конфигураций устройства, толщины полупроводника, сотрудничающего материала, уровня добавок и омовых контактов. В конце вычислены выход тока и абсолютная производительность переработки солнечных батарей с Zn_3P_2. Полученные результаты вычислений сравнены с экспериментальными данными для первообразных устройств.